ISSN: 2639-7536

Research Article

Petroleum and Chemical Industry International

Design and Simulation of Plasmonic Sensor by Changing the Refractive Index and Based on a Resonance System Using Two Rings, Two Cavities and Two Plasmonic Waveguides

Hamid Abbasi*

University of Mazandaran, Iran

***Corresponding Author**
Hamid Abbasi, University of Mazandaran, Iran.

Submitted: 2023, July 15; **Accepted**: 2023, Aug 10: **Published**: 2023, Aug 16

Citation: Abbasi, H. (2023). Design and Simulation of Plasmonic Sensor by Changing the Refractive Index and Based on a Resonance System Using Two Rings, Two Cavities and Two Plasmonic Waveguides. *Petro Chem Indus Intern, 6(*4), 248-260.

Abstract

In this research, we will design and numerically evaluate a plasmonic sensor based on the resonance system along with the metal-insulated metal waveguide (MIM). The structure of this sensor forms a wide range of wavelengths by changing the refractive index. To design the structure of this sensor, we use two cavities, two plasmonic waveguides and two rings with different dimensions. After designing the sensor structure, we examine the resonant wavelengths and refractive index of the resonators. For this purpose, we use the finite difference method of the time domain, because this method directly obtains Maxwell's equations with proper separation in the two domains of time and space and tells us how to properly design the dimensions and coordinates of the sensor structure and get a good result. At the beginning of the simulation, an electromagnetic wave is sent to the sensor structure to analyze the field distribution and the spectral response of the structural parameters. If the field distribution in the structure is the same, the energy loss is reduced and all dimensions must be optimal to reach the maximum field distribution in the structure. The creation of surface plasmon resonance at the boundary of a metal surface and a dielectric material will increase the intensity of the electric field and correct the sensor performance. In this article, we need factors such as tunability in a range of wavelengths, S sensitivity coefficient, figure of merit (FOM), Q quality factor and width at half maximum value (FWHM) to measure the performance of the sensor. By increasing the number of amplifiers, the FWHM of the resonant wavelength can be modulated, and reach a sensitivity of 2713 nm/RIU is realized in the near-infrared region. We also draw all the diagrams of this sensor using MATLAB software.

Keywords: Optics, Plasmonics, Plasmon Surface Polaritons, Insulation Metal, Refractive Index Sensor.

1. Introduction

Optical integrated circuits are one of the most important tools for solving ambiguous issues in technology. To achieve integrated optical devices with high efficiency and reduction of barriers, we need to make plasmonic structures small and compact. Plasmonic science, in short, means the interaction of radiation electromagnetic waves with the surface of metals and their conducting electrons and limiting electromagnetic waves in dimensions much smaller than the radiation wavelength. If plasmonics is divided into two parts, surface plasmon polaritons and localized surface plasmons, In this paper, we use surface plasmon polariton (SPP) because they can overcome the limitation of classical optical diffraction and act as energy carriers in circuits and optical devices [6-8]. Also, two types of popular SPP structures are metal-insulator-metal (MIM) and insulator-metal-insulator (IMI) structures (such as filters, couplers, sensors, etc....). In this article, the structure of metal insulating metal (MIM) because they have supporting modes, high group speed, very high optical confinement and acceptable propagation length. The most important plasmonic components are based on the structure of active (anisotropic) and passive (isotropic) environments. In this article, we use active environments because by applying an external factor, you can change their refractive index and wavelength. That is, active environments are suitable for switches and sensors. To make quality sensors, we need to consider parameters such as high transmission efficiency, high quality factor, high resolution, sensitivity enhancement and adjustability in a range of wavelengths. Improving these parameters will strengthen and increase the speed of information processing in optical integrated circuits. In this article, we use a set of metal-dielectricmetal (MIM) waveguides and plasmonic resonators to design and build the desired sensor. Also, we only change the refractive index of one structure and the rest of the structures will have a fixed refractive index. The purpose of this work is to challenge the quality of the sensor and achieve the best type of sensor performance [9-19].

2. Structural Model Design and Experimental Theory Analysis

Each waveguide with any kind of geometric shape can transmit waves and limit their energy in one and two dimensions. Of course, the geometry of the waveguide indicates its performance, and the frequency of the transmitted wave determines the size of a waveguide. Wave transmission is interpreted by the wave equation. Also, Maxwell's equations describe the shape of electromagnetic cross waves, and the equation of linear electricity describes the shape of sound waves. Using Maxwell's equations and the plasma model, the optical properties of metals can be explained [20]. When metals acquire dielectric properties, they can be interpreted using the plasma model (Drude model):

$$\varepsilon(\omega) = \varepsilon_{\infty} - \frac{{\omega_p}^2}{\omega^2 + i\gamma\omega} \qquad (1)$$

ω is the angular frequency, ∞ = 1 is the dielectric constant of infinite frequency, ωp = 1.37 × 1016 is the plasma frequency and γ = 3.21 × 1013 is the electron oscillation frequency. The Drude model provides a microscopic description of metal dynamics in the form of classical sentences. To design the desired sensor and check its performance, we add rings and cavities to the simulation respectively. The proposed structure is shown in Fig.1, which consists of two waveguides and a ring located in the middle of the two waveguides. The ring has an inner radius of r_1 = 95 nm and an outer radius of R_1 = 133 nm and its distance from the two waveguides is 12 nm. The height of the two waveguides is w_1 = 50 nm and the input wave goes from the left waveguide to the structure and after passing through it goes to the output waveguide. Pin and Pout are monitors for measuring input and output waves, respectively. The wave transfer is calculated by the following equation:

$$T = \frac{P_{out}}{P_{in}} \qquad (2)$$

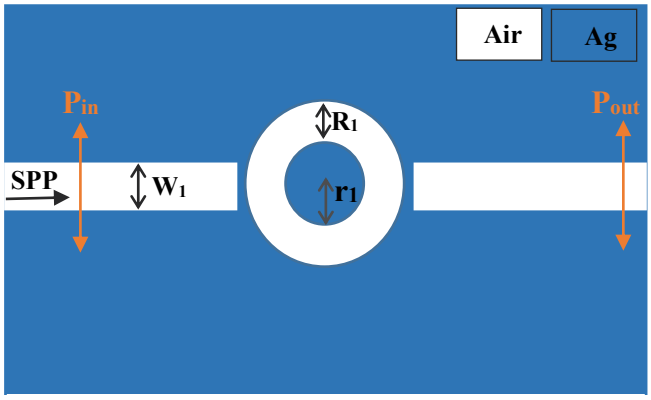

Figure 1: Two-dimensional image of a plasmonic sensor.

The simulation substrate is made of silver and the internal environment of the resonators is made of air. Because the wavelength of the radiation light is larger than the width of the waveguides, only the TM mode exists in the sensor structure. According to Fig.1, the TM wave with a strong magnetic field intensity moves from the left side and propagates in the waveguide to reach the end of the path. As this TM wave gets closer to the output part, its intensity decreases and each of the resonators reflects a part of the input wave. The dispersion relation of this fundamental state is expressed as follows [21]:

$$\frac{\varepsilon_i\, p}{\varepsilon_m k} = \frac{1 - e^{kw}}{1 + e^{kw}} \qquad (3)$$

$$k = k_0 \sqrt{\left(\frac{\beta_{sp}}{k_0}\right)^2 - \varepsilon_i} \qquad (4)$$

$$p = k_0 \sqrt{\left(\frac{\beta_{sp}}{k_0}\right)^2 - \varepsilon_m} \qquad (5)$$

$$\beta_{sp} = n_{eff} k_0 = n_{eff} \frac{2\pi}{\lambda} \qquad (6)$$

Here ω refer to the width of bus waveguide, λ shows incident light wavelength in vacuum, ε_i and ε_m give the relative dielectric and metal permittivity, β_{spp} and n_{eff} are propagation constant and effective refractive index of SPPs, and $=2\pi/\lambda$ k_0 means wave number. In most of the designed plasmonic sensors use two-dimensional simulation to test the performance of devices.

3. Implementation of Simulation Methods and Measurement of Refractive Index

To numerically investigate the resonant behaviour of the proposed sensor, we use the finite difference time domain (FDTD) simulation method. This method makes the input wave has less reflection. Also, this method has perfectly matched layer (PML) boundary conditions. To start the simulation, we need to select the mesh size. After doing the calculations and changing the mesh, we come to the conclusion that the size of the uniform mesh for the x and y directions is 8 nm (Fig.2). Because here, the height and number of peaks are more regular and the amount of wavelength change is greater (the mesh has suitable oscillation and noise).

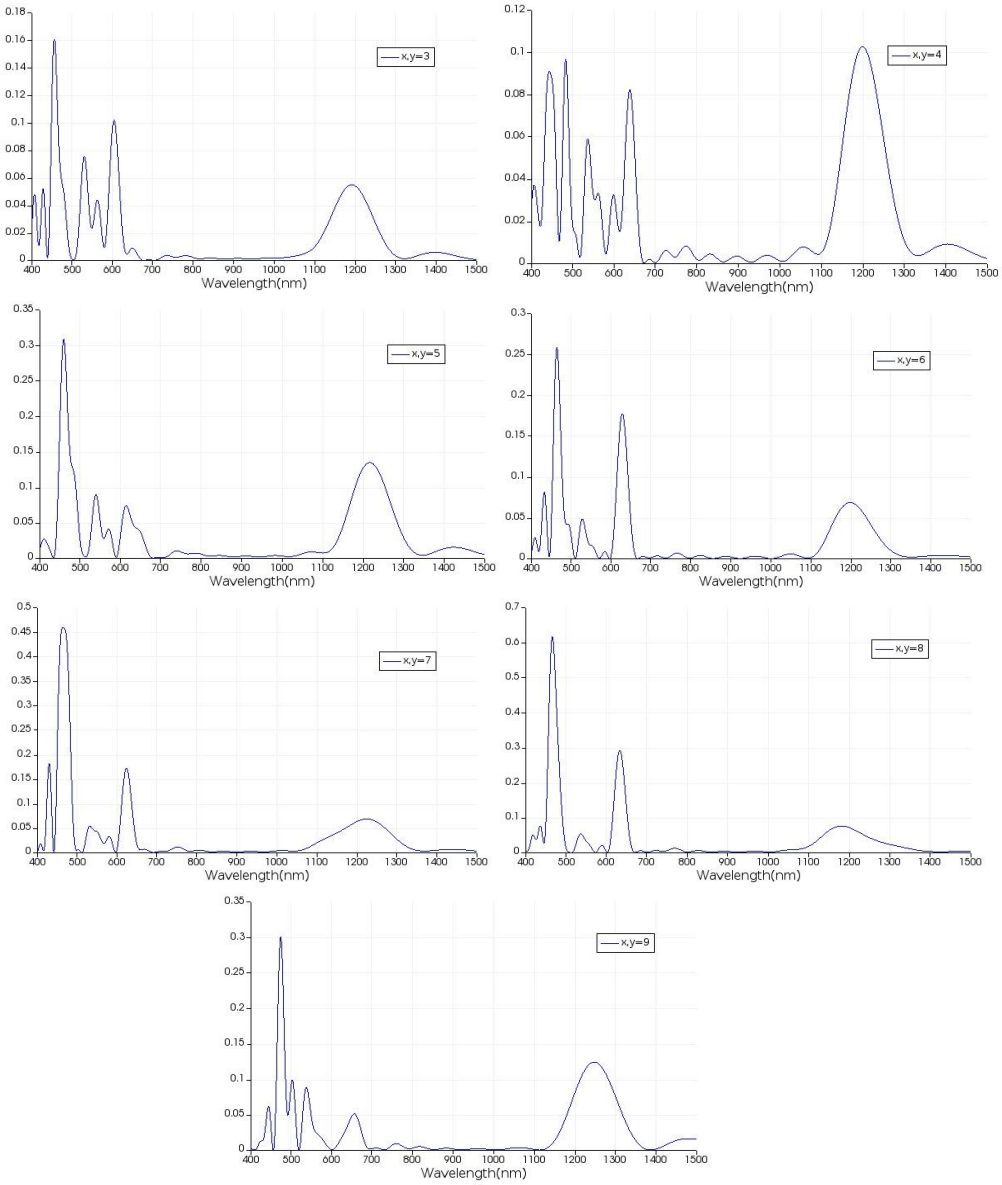

Figure 2: Diagram of changing meshes.

To reduce the simulation time and design the sensor structure more accurately, we perform the simulation in two dimensions. We also use the transmission line model to analyse the sensor structure theory. We change the refractive index of the sensor to obtain the wavelength change in the range of 400-1500 nm, and then plot the transmission spectrum of the sensor device to check the obtained modes from the transmission. According to Fig.3, the transmission spectra of the sensor have three peaks. The left and middle peaks have a higher height and narrower FWHM, but the amount of resonance wavelength change in these two peaks is low, and the peak on the right has a greater change in wavelength. The most important factor to check the performance of plasmonic sensor is the sensitivity, which is obtained by

equation (7):

$$S = \frac{\Delta \lambda}{\Delta n} \quad (\mathrm{nm/RIU}) \qquad (7)$$

In this equation, $\Delta\lambda$ is the change in resonance wavelength and Δn is the change in refractive index.

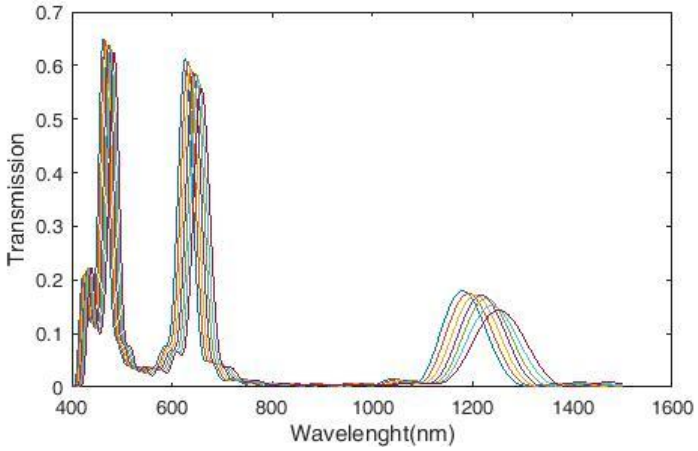

Figure 3: Transmission spectra of plasmonic refractive index sensor

In this simulation, we change the refractive index of the middle ring with steps of 0.01 nm from n = 1.07 to n = 1.13. Using Fig.4, we plot the number of changes in the refractive index for the change in the resonance wavelength, and by examining it, we come to the conclusion that there is a linear relationship between the two parameters of the resonance wavelength and the refractive index of the sensor, and the TM wave resonance gradually shifts. According to Figures 3 and 4, we conclude that the peaks on the left and middle have less fluctuation and the change in wavelength affects them regularly, but the peak on the right has more fluctuation and turbulence, and Changing the wavelength transfers more energy to it.

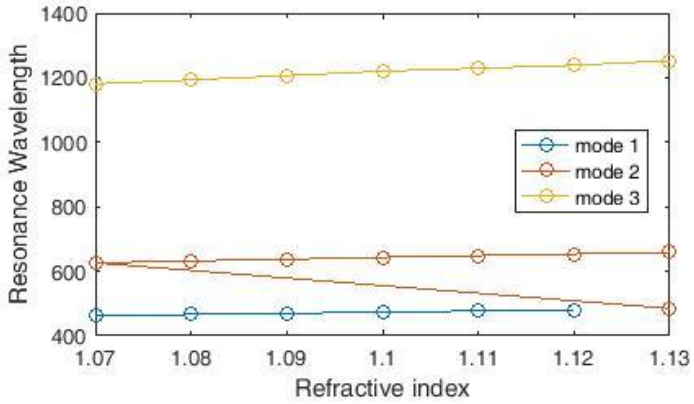

Figure 4: Resonance wavelength versus refractive index changes.

As a result, using Equation 7, we obtain the sensitivity of different wavelengths. According to Fig.5, the maximum sensitivity for the refractive index is n = 1.13 (in mode3), which is equal to 1424 nm / RIU, and the lowest value is for the refractive index n = 1.08 (in mode1), which is equal to 330.2.

Therefore, mode 3 is more sensitive than mode1 and mode2.

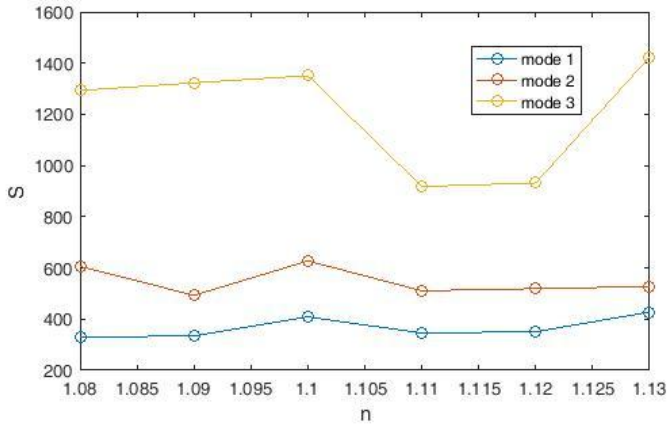

Figure 5: Plasmonic sensor sensitivity coefficient diagram.

Since the sensitivity factor alone cannot fully evaluate the performance of the sensors, we need two other factors, namely the Q quality factor and figure of merit (FOM). Increasing the length of the resonators improves the sensor performance, and the lengthening of the optical path and more energy loss increases the sensitivity and reduces the figure of merit (FOM). Therefore, the second factor to check the sensor performance is the figure of merit (FOM), which is obtained from equation (8):

$$FOM = \frac{S}{FWHM} \qquad (8)$$

Using equation (8), we plot the figure of merit (FOM) diagram and by examining it, we come to the conclusion that the maximum value for the figure of merit (FOM) in the refractive index is n = 1.13 (in mode 1), which is equal to 17.259 nm / RIU (Figure 6). We also conclude that mode 1 has higher figure of merit (FOM) and mode 3, which had a higher sensitivity coefficient, has smaller figure of merit (FOM).

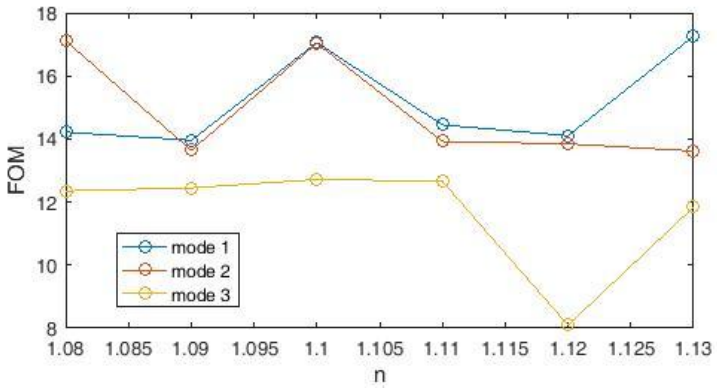

Figure 6: Figure of merit (FOM) diagram of plasmonic sensor

The third factor to check the sensor performance is the quality coefficient Q, which is obtained by dividing the wavelength by the FWHM (Equation 9):

$$Q = \frac{\lambda_{res}}{FWHM} \qquad (9)$$

The diagram of the quality coefficient is obtained using equation 9 (Figure 7), the highest value of which corresponds to the refractive index n = 1.08 (in mode 1), which is equal to 20.072 nm / RIU, and the lowest value is for the refractive index n = 1.13 (in mode 3), which is equal to 10.416 nm / RIU. Examining these three factors shows that our proposed sensor has the highest fluctuation at the refractive index n = 1.08 and the sensor will have the highest resonance at this point. For further investigation, we obtain the field distribution at this point.

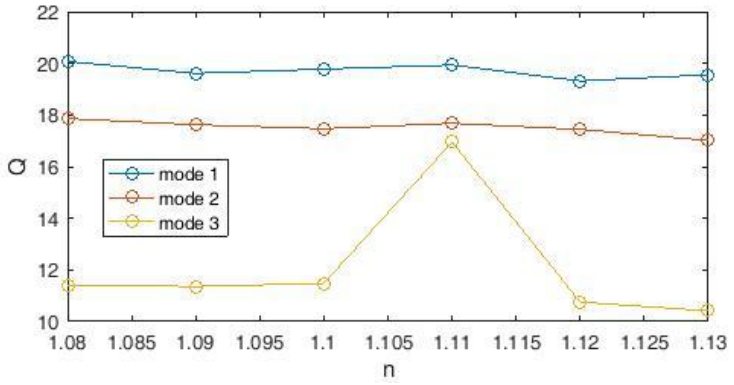

Figure 7: Diagram of quality coefficient Q of plasmonic sensor

According to Fig.8, the incoming wave covers the entire ring and the field distribution is regular on the inner surface of the ring

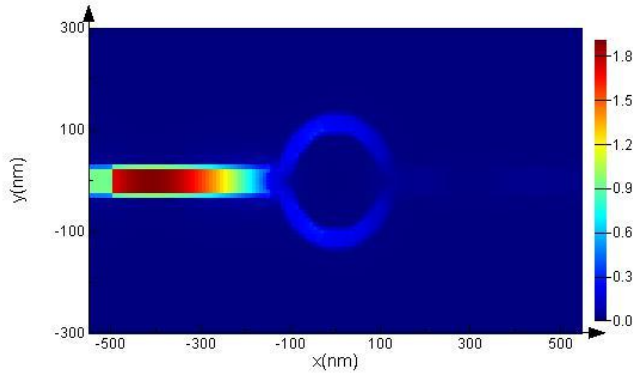

Figure 8: Field distribution diagram in plasmonic sensor

4. Plasmonic Sensor with Two Waveguides, Two Rings and a Cavity

We add a ring with inner radius r2=80 nm and outer radius R2=120 nm and a cavity with length L1=92 nm and height W2=200 nm to the sensor structure and create a new structure (Fig.9). This ring and the cavity that are stuck together are located at the bottom of the right waveguide.

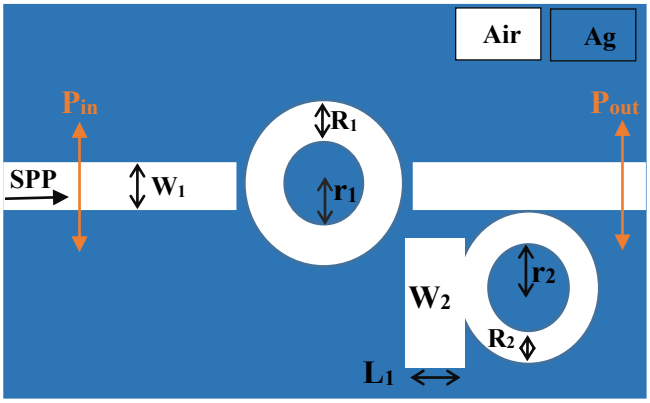

Figure 9: Plasmonic sensor with two waveguides and two rings and a cavity.

To measure the sensor performance and calculate the sensitivity, figure of merit (FOM) and quality factor Q in this new structure, we only change the refractive index of the middle ring and the refractive index of the other resonators remains the same. This makes the sensor structure experience more challenges and achieve more accurate results. Next, we change the refractive index of the sensor in the wavelength range of 400-1500 nm to obtain the resulting transmission spectrum (Fig.10). Three peaks are obtained, the left peak and the middle peak have a higher height and a narrower FWHM than the right peak. But the peak on the right has a greater wavelength change than the other two peaks.

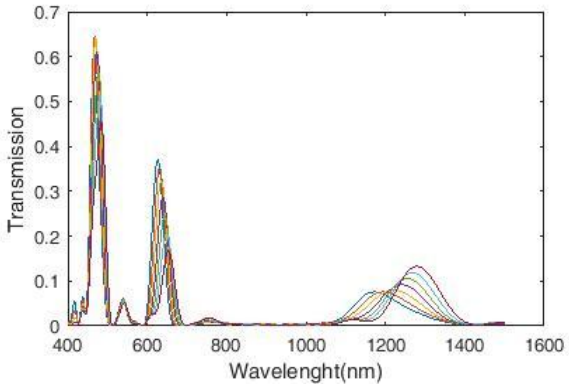

Figure 10: Plasmonic sensor transmission spectra with two waveguides, two rings and a cavity

Also, the peak on the right in Fig.10 has a wider FWHM and a greater wavelength change than the peak on the right in Fig.3. This means that the structure of Fig.9 has a higher sensitivity than the structure of Fig.1. If we check the number of changes in the refractive index in the selected wavelength range for the structure of Fig.9 and plot a diagram for it (Fig.11), we will come to the conclusion that peak 3 has better conditions than the other two peaks and the amount of length shift The wave in this peak is higher than the other two peaks.

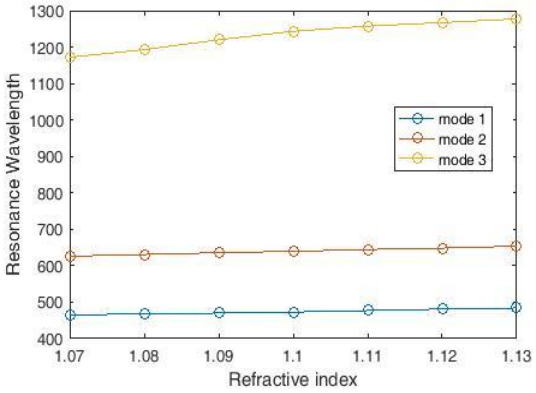

Figure 11: Resonance wavelength versus refractive index changes.

Using Fig.11 and Equation (7), we get the sensitivity of different wavelengths. According to Fig.12, the highest sensitivity is for the refractive index n = 1.09 (in mode 3), which is equal to 2673 nm / RIU, and the lowest value is for the refractive index n = 1.08 (in mode 1), which is equal to 199 nm / RIU. This means that by adding resonators, waves and waveguides are more affected and we reach more sensitivity.

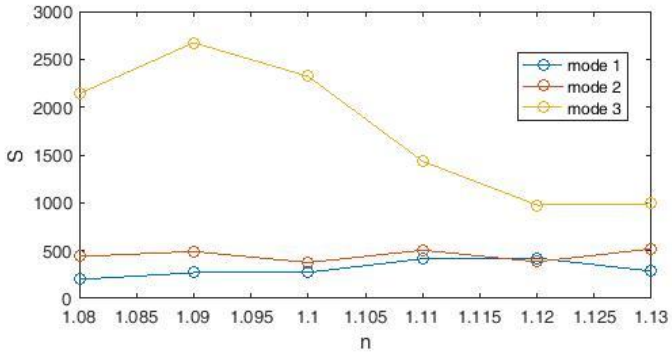

Figure 12: Plasmonic sensor sensitivity coefficient diagram with two waveguides, two rings and a cavity.

Using Fig.12 and Equation (8), we calculate the figure of merit (FOM) and plot its graph (Fig.13). According to the figure, Peak 1 has less FOM and peaks 2 and 3 have more FOM changes and as a result have more dependence on wavelength change. As a result, the highest value of the figure of merit (FOM) for the refractive index is n = 1.09 (in mode 3), which is equal to 17.049 nm / RIU.

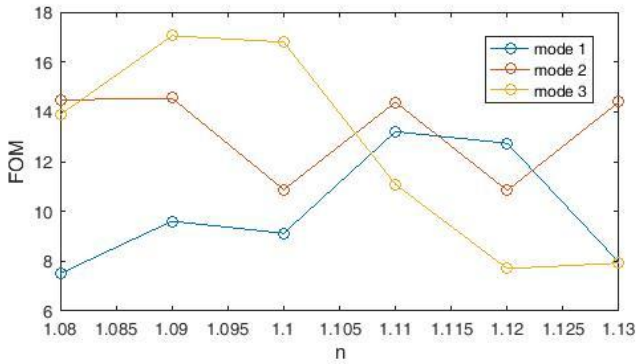

Figure 13: Figure of merit (FOM) diagram of plasmonic sensor with two waveguides, two rings and one cavity.

Using equation (9), we calculate the quality coefficient Q of this sensor and plot its diagram (Fig.14). The highest value of the quality coefficient Q corresponds to the refractive index n = 1.08 (in mode 2), which is equal to 18.887 nm / RIU, and the lowest value is for the refractive index n = 1.08 (in mode 3), which is equal to 7.74 nm. / RIU.

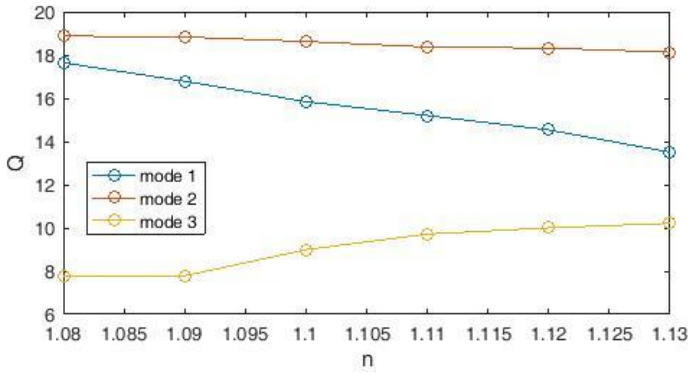

Figure 14: Diagram of quality coefficient Q of plasmonic sensor with two waveguides, two rings and one cavity.

5. Plasmonic Sensor With Two Waveguides, Two Rings and Two Cavity

Next, we add a cavity with length L2=92 nm and height W3=200 nm to the left side of the structure (Fig.15). The distance between the two cavities is 278 nm and their distance from the waveguides is 42 nm. Naturally, the sensor structure experiences a new challenge, so we re-evaluate and review the sensor performance.

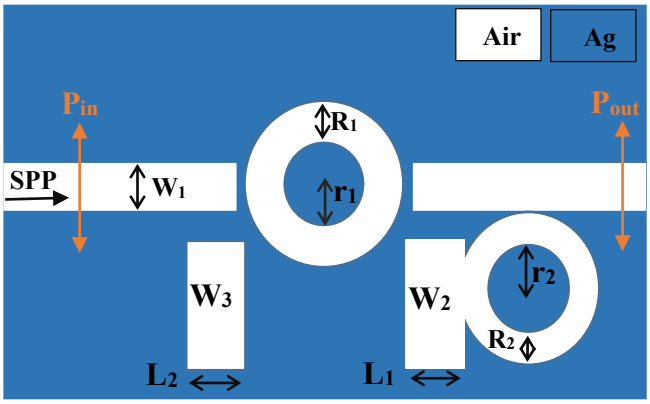

Figure 15: Two-dimensional image of a plasmonic sensor with two waveguides, two rings and two cavities.

As in the previous simulations, we only change the refractive index of the middle ring in the wavelength range of 400-1500 nm and keep the refractive index of other resonators constant. As a result, we get the resulting transmission spectrum (Fig.16). According to the figure, the left peak has the highest height and the middle peak has the narrowest FWHM. But the side peak has a lower height and a wider FWHM.

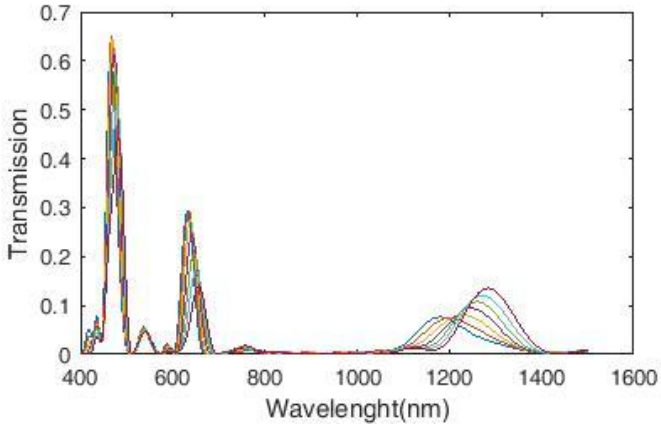

Figure 16: Plasmonic refractive index sensor transmission spectra with two waveguides, two rings and two cavities.

Also, the peak on the right in Fig.16 has a wider FWHM and a greater wavelength change than the peak on the right in Figures 3 and 10. This means that the structure of Fig.10 has a higher sensitivity than the structure of Figures 1 and 9, and the designed sensor will perform better. Our purpose of adding the resonators step by step, was to measure their position and choose the most suitable dimensions for them. Now we check the number of changes in the refractive index in the selected wavelength range for the new structure and plot the corresponding graph (Fig.17). As before, it is proved that there is a linear relationship between the resonance wavelength and the refractive index. According to the figure, The peak on the right has a greater wavelength change compared to the other two peaks as well as the peaks of the previous two structures and as a result, it has a higher sensitivity.

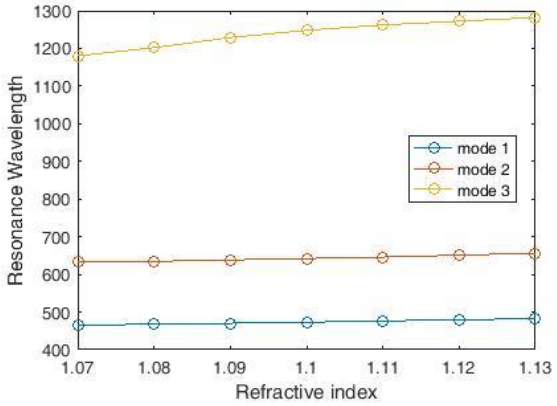

Figure 17: Resonance wavelength versus refractive index changes.

To calculate the sensitivity of the sensor, we use equation (7). According to Fig.18, the highest sensitivity is for the refractive index n = 1.09 (in mode 3), which is equal to 2713 nm / RIU, and the lowest value is for the refractive index n = 1.08 (in mode 1), which is equal to 199.9 nm. An important point in simulating this sensor is the selection of resonators whose refractive index changes. If in this simulation, we only change the refractive index of the middle ring, we will reach a higher sensitivity than when the refractive index of all resonators is changed.

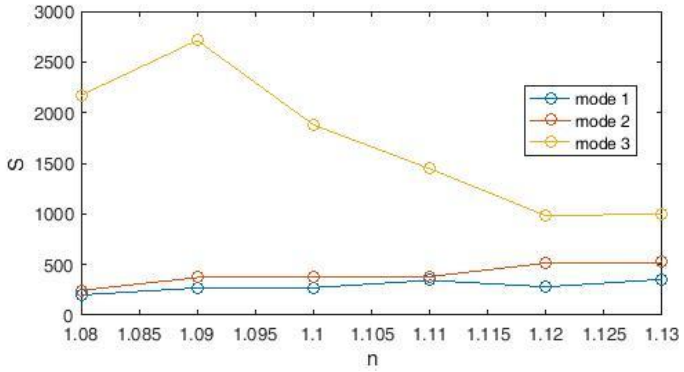

Figure 18: Plasmonic sensor sensitivity coefficient diagram with two waveguides, two rings and two cavities.

Now we have to calculate the figure of merit (FOM) and draw its diagram (Fig.19). The figure of merit of (FOM) in refractive index n = 1.09, which has the highest sensitivity coefficient, reaches the value of 18.669. Like the sensitivity factor, the figure of merit of (FOM) has also increased compared to the previous structure.

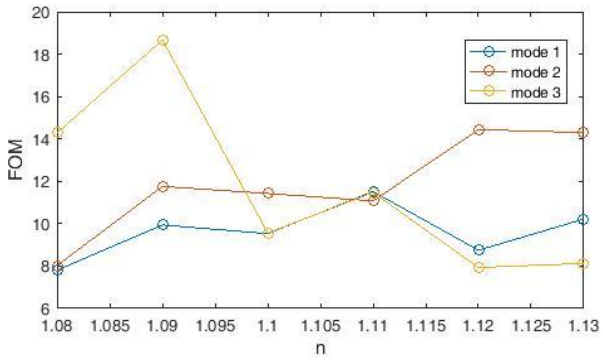

Figure 19: Diagram of the figure of merit (FOM) of a plasmonic sensor with two waveguides, two rings and two cavities.

The last criterion for measuring this sensor is the quality coefficient Q, whose graph is obtained using equation 9 (Fig.20). The value of the quality coefficient Q in the refractive index n = 1.09, which has the highest sensitivity, reaches the value of 8.458.

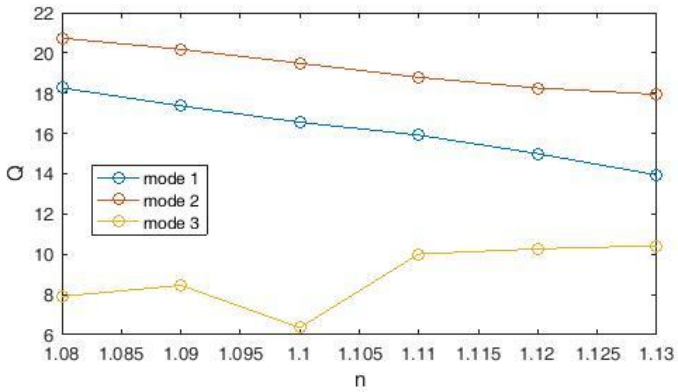

Figure 20: Quality coefficient diagram of Q plasmonic sensor with two waveguides, two rings and two cavities.

The Sensor field distribution when it reaches its highest sensitivity value, i.e. 2713 nm/RIU, can be seen in Fig.21. Field distribution in rings is stronger than two cavities. Also, the middle ring has a stronger field distribution than the right ring, and it has the highest field distribution and creates the transfer slope.

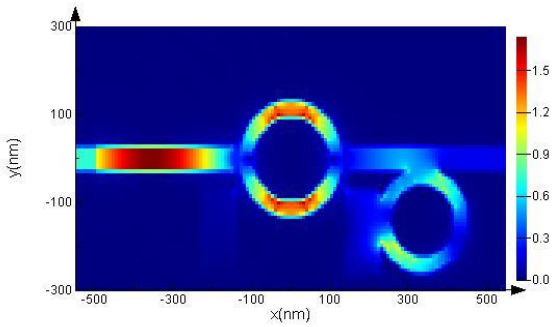

Figure 21: Plasmonic sensor field distribution.

As shown in Table 1, the proposed method for making the desired sensor provides better results compared to some similar articles. According to this table, the maximum value of sensitivity among these articles belongs to the structure investigated in this article, which is equal to 2713 nm.

Conclusion

Plasmonic sensors are a vast and important topic in scientific research and we have revealed the latest developments in the design of these sensors, based on metal-insulator plasmonic waveguides. The structure of the sensor was analysed numerically and theoretically, and its results were obtained using the transmission line model and the time domain finite difference method. The theoretical results agree with the numerical results. We have achieved sensitivities of 2713 nm/RIU and 2673 nm/RIU in several plasmonic resonator designs discussed. This proposed device can be used in plasmonic sensing systems in the infrared region and improve the performance of sensors that will be designed in the future.

ReferenceS	Topology	Resonance wavelength (nm)	FOM (RIU^{-1})	S (nm/RIU)
Bahramipanah et al. (2014)	Loop shaped stub	1550	31.4	1132
Yan et al. (2015)	Ring resonator	887	43.9	868
Zafar and Salim(2015)	Toothshaped stubs	1000	176.7	1060
Chen and Yao(2016)	Sidecoupled Waveguide resonator	1050	28.2	985
Zhang et al. (2016)	Double rectangular cavities	620	7.5	596
Akhavan et al. (2017)	Coupled double rectangular cavities	826	31.6	860
Tang et al. (2017)	Rectangular and ring resonators	1010	75	1125
Wu et al. (2018)	Sidecoupled Hexagon resonators	571	178	560
Akhavan et al. (2018)	Double sidecoupled square ring resonators	826	66	806

Zhang et al. (2018)	Concentric double Rings resonator	The near infrared region	1060	203.8
Wang et al. (2018)	T shaped resonator	682	8.68	625
Rafiee et al. (2019)	Square type split-ring resonator	980	24.3	1217
Danaie and Shahzadi. (2019)	Si ring resonator	808	211.3	636
M.Danaie et (al. 2020)	Cascaded coupled concentric ring and disk resonator	650	287.9	640.6 for six resonators
This work	Two plasmonic waveguides, two ring and two cavities	1229.14	18.669	2713

Table 1: Comparison between proposed sensor specifications and similar articles.

Funding
This research received no external funding.

Conflicts of Interest
The authors declare no conflict of interest.

Availability of Data and Material
All materials and data of this article are at the disposal of the authors.

References

1. Zhang, Z., Zhang, S., Liu, Y., & Xiong, Z. (2011). Cascade electric field enhancement in the orthogonal-nanorod structures. Plasmonics, 6, 177-182.
2. Zhang, Z. D., Wang, H. Y., & Zhang, Z. Y. (2013). Fano resonance in a gear-shaped nanocavity of the metal–insulator–metal waveguide. Plasmonics, 8, 797-801.
3. Li, H., Xu, Y., Wang, G., Fu, T., Wang, L., & Zhang, Z. (2017). Converting surface plasmon polaritons into spatial bending beams through graded dielectric rectangles over metal film. Optics Communications, 383, 423-429.
4. Li, N., Tian, X., Zhang, W., Luo, L., Li, G., & Zhang, Z. (2015). Double Fano resonances in a planar pseudo-dolmen structure. Sensors and Actuators A: Physical, 234, 346-350.
5. Yan, Z., Wen, X., Gu, P., Zhong, H., Zhan, P., Chen, Z., & Wang, Z. (2017). Double Fano resonances in an individual metallic nanostructure for high sensing sensitivity. Nanotechnology, 28(47), 475203.
6. Cen, C., Lin, H., Huang, J., Liang, C., Chen, X., Tang, Y., ... & Xiao, S. (2018). A tunable plasmonic refractive index sensor with nanoring-strip graphene arrays. Sensors, 18(12), 4489.
7. Cheng, F., Yang, X., & Gao, J. (2014). Enhancing intensity and refractive index sensing capability with infrared plasmonic perfect absorbers. Optics letters, 39(11), 3185-3188.
8. Cheng, L., Wang, Z., He, X., & Cao, P. (2019). Plasmonic nanosensor based on multiple independently tunable Fano resonances. Beilstein journal of nanotechnology, 10(1), 2527-2537.
9. Wu, W., Yang, J., Zhang, J., Huang, J., Chen, D., & Wang, H. (2016). Ultra-high resolution filter and optical field modulator based on a surface plasmon polariton. Optics letters, 41(10), 2310-2313.
10. Zhang, L., Pan, C., Zeng, D., Yang, Y., Yang, Y., & Ma, J. (2020). A hybrid-plasmonic-waveguide-based polarization-independent directional coupler. IEEE Access, 8, 134268-134275.
11. Liang, C., Niu, G., Chen, X., Zhou, Z., Yi, Z., Ye, X., ... & Xiao, S. (2019). Tunable triple-band graphene refractive index sensor with good angle-polarization tolerance. Optics Communications, 436, 57-62.
12. Liu, C., Su, W., Liu, Q., Lu, X., Wang, F., Sun, T., & Chu, P. K. (2018). Symmetrical dual D-shape photonic crystal fibers for surface plasmon resonance sensing. Optics express, 26(7), 9039-9049.
13. Liu, Z., Yu, M., Huang, S., Liu, X., Wang, Y., Liu, M., ... & Liu, G. (2015). Enhancing refractive index sensing capability with hybrid plasmonic–photonic absorbers. Journal of Materials Chemistry C, 3(17), 4222-4226.

14. Yun-Ping, Q., Xue-Wei, Z., Pei-Yang, Z., Bing-Bing, H., & Xiang-Xian, W. (2018). Refractive index sensor and filter of metal-insulator-metal waveguide based on ring resonator embedded by cross structure.
15. Cen, C., Lin, H., Huang, J., Liang, C., Chen, X., Tang, Y., ... & Xiao, S. (2018). A tunable plasmonic refractive index sensor with nanoring-strip graphene arrays. Sensors, 18(12), 4489.
16. Liu, C., Yang, L., Lu, X., Liu, Q., Wang, F., Lv, J., ... & Chu, P. K. (2017). Mid-infrared surface plasmon resonance sensor based on photonic crystal fibers. Optics express, 25(13), 14227-14237.
17. Chen, L., Liu, Y., Yu, Z., Wu, D., Ma, R., Zhang, Y., & Ye, H. (2016). Numerical analysis of a near-infrared plasmonic refractive index sensor with high figure of merit based on a fillet cavity. Optics express, 24(9), 9975-9983.
18. Tong, L., Wei, H., Zhang, S., & Xu, H. (2014). Recent advances in plasmonic sensors. Sensors, 14(5), 7959-7973.
19. Shen, Y., Zhou, J., Liu, T., Tao, Y., Jiang, R., Liu, M., ... & Wang, J. (2013). Plasmonic gold mushroom arrays with refractive index sensing figures of merit approaching the theoretical limit. Nature communications, 4(1), 2381.
20. Maier, S. A. (2007). Plasmonics: fundamentals and applications (Vol. 1, p. 245). New York: springer.
21. Maier, Stefan A. Plasmonics: Fundamentals and Applications. Springer Berlin 2014, 52.11, 49-74.